Solid State Communications 193 (2014) 51–55

Contents lists available at ScienceDirect

Solid State Communications

journal homepage: www.elsevier.com/locate/ssc

Signatures of the spin-phonon coupling in $Fe_{1+y}Te_{1-x}Se_x$ alloys

Z.V. Popović [a,*], N. Lazarević [a], S. Bogdanović [a], M.M. Radonjić [b], D. Tanasković [b], Rongwei Hu [c,1], Hechang Lei [c,2], C. Petrovic [c]

[a] Center for Solid State Physics and New Materials, Institute of Physics Belgrade, University of Belgrade, Pregrevica 118, 11080 Belgrade, Serbia
[b] Scientific Computing Laboratory, Institute of Physics Belgrade, University of Belgrade, Pregrevica 118, 11080 Belgrade, Serbia
[c] Condensed Matter Physics and Materials Science Department, Brookhaven National Laboratory, Upton, New York 11973-5000, USA

ARTICLE INFO

Article history:
Received 30 December 2013
Received in revised form
28 April 2014
Accepted 28 May 2014
by M. Wang
Available online 10 June 2014

Keywords:
A. Magnetically ordered materials
C. Crystal structure and symmetry
D. Phonos
E. Inelastic light scattering

ABSTRACT

Raman scattering spectra of $Fe_{1+y}Te_{1-x}Se_x$ ($x=0$, $y=0.07$; $x=0.1$, $y=0.05$ and $x=0.4$, $y=0.02$) alloys are measured in a temperature range between 20 K and 300 K. The A_{1g} and B_{1g} Raman active modes have been experimentally observed at energies 156 and 198 cm^{-1}, which is in rather good agreement with the lattice dynamics calculation. The antiferromagnetic spin ordering below 70 K in $Fe_{1.07}Te$ leaves a fingerprint only in the B_{1g} phonon mode linewidth and energy, whose temperature dependence follows the normalized magnetic susceptibility, indicating the presence of the spin-phonon coupling. The frequency and the linewidth of the A_{1g} mode assume a conventional anharmonic temperature dependence in all measured samples, which is also the case for the B_{1g} mode in the Se doped samples. The linewidth (energy) of the A_{1g} mode decreases (increases) with doping, whereas the opposite is seen for the B_{1g} mode.

1. Introduction

The discovery of a new $LaFeAsO_{1-x}F_x$ superconductor family with $T_c=24$ K spurred the research in the field of iron-based superconductors [1–3]. Among these compounds, iron-chalcogenides have the simplest crystal structure of the PbO type including only Fe and Ch atoms (Ch=S, Se and Te) [4,5]. This structure consists of Fe square planar sheets with Ch ions forming distorted tetrahedra around the Fe ions, analogous to the structure of the FeAs planes in LaFeAsO, $BaFe_2As_2$, and LiFeAs, which are prototypes of the known families of Fe–As based high-T_c superconductors [6–8]. In fact, these structures match the reported structure of $K_xFe_{2-y}Se_2$ with interspersed FeSe stacked along the *c*-axis [9,10].

FeTe crystallizes in the tetragonal system of the *P4/nmm* space group [11]. By lowering the temperature below 70 K, there is a structural transition from the tetragonal to the monoclinic lattice ($P2_1$/m space group), accompanied by the antiferromagnetic spin ordering [12]. Partial substitution of Te with Se progressively suppresses the magnetic ordering temperature and structural transition [13], and leads to the superconductivity at low temperatures [11]. The T_c of the $Fe_{1+y}Te_{1-x}Se_x$ system can reach up to 14 K at ambient pressure for $x=0.5$ [14] and 27 K at a pressure of 1.46 GPa [15].

The mechanism for superconductivity in the iron-based materials is still under debate [16]. In particular, the magnetic ordering and spin fluctuations are expected to have an important impact on the phonon dynamics and lead to the increase of the electron–phonon coupling [17] which is, however, still insufficient to explain high T_c in these compounds.

Raman scattering is an excellent tool for a study of the phonon properties of materials and its coupling to the electronic charge and spin excitations. Although the Raman scattering spectra in $Fe_{1+y}Te_{1-x}Se_x$ alloys were analyzed in Refs. [18–21], there are several features in the spectra that have not been fully resolved and understood. Two modes at about 155($\pm$4) and 199($\pm$3) cm^{-1} are experimentally observed and assigned as the A_{1g} (Te-ions vibration along the *z*-axis) and the B_{1g} (Fe-ions vibration along the *z*-axis) modes, respectively. Calculated phonon frequencies of these modes agree with the experimental data within 10%, see Table 1. The temperature dependence of the phonon mode linewidth and energy of undoped FeTe sample is, however, controversial. Gnezdilov et al. [20] found an increase of the A_{1g} mode linewidth from 28 to 31.4 cm^{-1} by lowering the temperature from 200 K to 5 K. This A_{1g} mode temperature dependence deviates from the anharmonic picture. In addition, they found the A_{1g} mode energy change about the phase transition temperature

* Corresponding author. Tel.: +381 11 3161385.
[1] Present address: Department of Physics, University of Maryland, College Park, MD 20742-4111, USA.
[2] Present address: Frontier Research Center, Tokyo Institute of Technology, 4259 Nagatsuta, Midori, Yokohama 226-8503, Japan.

http://dx.doi.org/10.1016/j.ssc.2014.05.025
0038-1098/© 2014 Elsevier Ltd. All rights reserved.

Table 1
Calculated and experimentally observed values of the Raman active phonon mode energies (in cm^{-1}) of FeTe single crystal in tetragonal (upper part of the table) and monoclinic (lower part of the table) phase.

Symmetry	Calculations				Experiment				
	Ref. [18]	Ref. [19]	Ref. [21]	This work	Ref. [18]	Ref. [19]	Ref. [21]	Ref. [20]	This work
Tetragonal phase (P4/nmm)									
E_g^1	59.1	120.1	–	**66.0**	–	–	–	–	
A_{1g}	140.3	168.4	175	**141.2**	159.1	158	159.7	151	**156**
B_{1g}	215.7	216.4	197.5	**214.7**	196.3	202	200.5	197	**198**
E_g^2	196.9	274.1	–	**215.2**	–	–	–	–	

Symmetry	Calculations		Experiment
	Ref. [20]	This work (nonmagnetic DFT)	This work
Monoclinic phase ($P2_1/m$)			
A_g^1	86.8	**67.8**	–
B_g^1	76.8	**69.2**	–
A_g^2	164.5	**141.0**	**160.5**
A_g^3	206.4	**204.8**	**200.2**
B_g^2	214.8	**218.7**	–
A_g^4	243.6	**222.3**	–

of T_N=70 K. Um et al. [21], on the other hand, found only minor A_{1g} mode broadening (from 19 to 21 cm^{-1} by lowering the temperature to 5 K) without the energy change at the phase transition temperature. The B_{1g} mode hardens and broadens with decreasing temperature down to T_N and then softens and narrows down to 5 K in both papers [20,21]. This feature is, however, supressed in the excess-Fe rich sample $Fe_{1.09}Te$ [21]. One additional mode at about 136 cm^{-1} for undoped FeTe sample is observed in Refs. [18,21], which origin is related to the sample decomposition.

In this paper we have measured the Raman scattering spectra of $Fe_{1+y}Te_{1-x}Se_x$ (x=0, y=0.07; x=0.1, y=0.05 and x=0.4, y=0.02) alloys in the temperature range from room temperature down to 20 K in the spectral range from 90 up to 300 cm^{-1}. In the optical phonon region of FeTe we have observed two optical phonons of the A_{1g} (156 cm^{-1}) and the B_{1g} (198 cm^{-1}) symmetries. The observed frequencies are in rather good agreement with our lattice dynamics calculations. The temperature dependence of the energy and linewidth of the B_{1g} mode in $Fe_{1.07}Te$ has a maximum at about T_N and follows the lineshape of the normalized magnetic susceptibility as seen in our magnetization measurements. Doping with Se suppresses T_N and a conventional temperature dependence is observed for the B_{1g} mode. We find that the energy and the linewidth of the A_{1g} mode assume a conventional anharmonic temperature dependence in all three samples. Phonon mode at 136 cm^{-1} is not observed in our samples. In Se doped samples the A_{1g} mode hardens and narrows, whereas the B_{1g} mode softens and broadens. These features cannot be simply explained just as a consequence of the substitution of Te by lighter and smaller Se ions and the disorder effect.

2. Experiment and numerical method

Single crystals of $Fe_{1+y}Te_{1-x}Se_x$ (x=0, y=0.07; x=0.1, y=0.05 and x=0.4, y=0.02) alloys were grown using self-flux method, as described in Ref. [22]. Raman scattering measurements were performed on freshly cleaved (001)-oriented samples using JY T64000 and Tri-Vista 557 Raman systems in backscattering micro-Raman configuration. The 514.5 nm line of an Ar^+/Kr^+ mixed gas laser was used as an excitation source. The corresponding excitation power density was less than 0.2 kW/cm^2. Low temperature measurements were performed using KONTI CryoVac continuous flow cryostat with 0.5 mm thick window. Magnetization measurements were carried out in Quantum Design MPMS-XL5 system.

We have calculated the lattice dynamics of both FeTe phases: the room temperature phase (tetragonal symmetry) and the low temperature phase (monoclinic symmetry). The lattice dynamics calculations are performed within the density functional perturbation theory (DFPT) [23] as implemented in the QUANTUM ESPRESSO package [24] using the generalized gradient approximation with the PW91 exchange-correlation functional which is used to obtain ultra-soft pseudo-potentials. Iron (tellurium) pseudo-potential includes $3s^2\ 4s^2\ 3p^6\ 4p^0\ 3d^6$ ($5s^2\ 5p^4\ 4d^{10}$) electron states for the valence electrons. The Brillouin zone is sampled with a Monkhorst-Pack 16 × 16 × 10 **k**-space mesh for higher-symmetry phase ($P4/nmm$ space group) and 16 × 16 × 8 **k**-space mesh for lower-symmetry phase ($P2_1/m$ space group). Unit cell is constructed using experimental values of the lattices parameters [25] ($P4/nmm$ phase: a=0.38219 nm, c=0.62851 nm; $P2_1/m$ phase: a=0.38312 nm, b=0.37830 nm, c=0.62643 nm and β=89.17degr). The Energy cutoffs for the wave functions and the electron densities are 64 Ry and 762 Ry, respectively, which are the highest suggested radii for the chosen pseudo-potentials. We have used Gaussian smearing of 0.001 Ry.

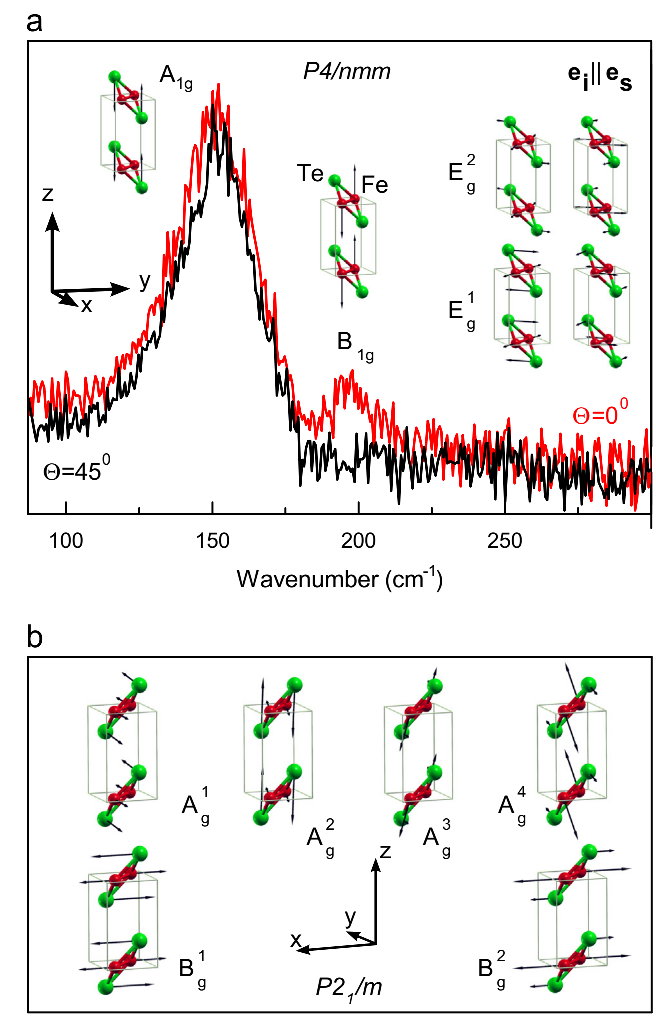

Fig. 1. (Color online) (a) Room temperature polarized Raman scattering spectra of the FeTe crystal (the tetragonal phase, space group *P4/nmm*) measured for different sample orientations together with normal modes. (b) The normal modes of lattice vibrations of the low temperature monoclinic phase of FeTe (the *P2₁/m* space group). The length of the arrows is proportional to the square roots of the vibration amplitudes.

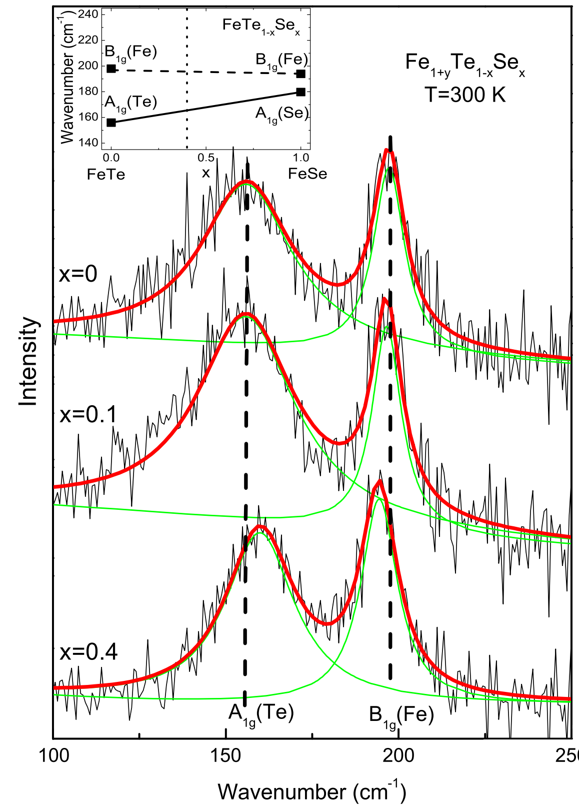

Fig. 2. (Color online) The unpolarized Raman scattering spectra of the (001)-oriented $Fe_{1+y}Te_{1-x}Se_x$ ($x=0$, $y=0.07$; $x=0.1$, $y=0.05$ and $x=0.4$, $y=0.02$) single crystals measured at room temperature. Red lines are calculated spectra obtained by Lorentzian line (green lines) profile fit. Inset: Experimental values (■) of the A_{1g} and B_{1g} modes of $FeTe_{1-x}Se_x$ for $x=0$ (this work) and $x=1$ (Ref. [33]). Solid and dashed lines represent linear fit between mode energies of parent materials.

3. Results and discussion

The results of the lattice dynamics calculations, together with the experimental data are presented in Table 1. Normal modes of Raman active phonons of both FeTe phases are given in Fig. 1.

Fig. 1(a) shows the polarized Raman scattering spectra of $Fe_{1.07}Te$ crystal measured from the (001) plane at room temperature in the spectral range from 90 to 300 cm^{-1}. Two peaks are observed at frequencies of about 156 and 198 cm^{-1}. According to the selection rules, when Raman scattering spectrum is measured from the (001) plane of the sample, only the A_{1g} and the B_{1g} modes can be observed. In the parallel polarization configuration ($\mathbf{e}_i \parallel \mathbf{e}_s$), the A_{1g} could be seen for an arbitrary orientation of the sample, whereas the B_{1g} mode vanishes for the sample orientation in which $\mathbf{e}_s \parallel \langle 110 \rangle$. By rotating the sample, we were able to find the orientation in which the peak around 198 cm^{-1} vanishes. Consequently, this peak is assigned as the B_{1g} symmetry mode, whereas the peak at around 156 cm^{-1} is assigned as the A_{1g} mode. This is in agreement with the previous assignment [18–21] and our lattice dynamics calculation (Table 1). The additional mode at about 136 cm^{-1}, as found in Ref. [21] for nearly stoichiometric $Fe_{1.02}Te$ sample, has not been observed in the spectra.

Fig. 2 shows the unpolarized Raman scattering spectra of $Fe_{1+y}Te_{1-x}Se_x$ ($x=0$, $y=0.07$; $x=0.1$, $y=0.05$ and $x=0.4$, $y=0.02$) single crystals measured at room temperature. Replacing Te with Se ions leads to the A_{1g} (the B_{1g}) mode hardening (softening), which is indicated in Fig. 2 where the vertical dashed lines denote the energies for the undoped sample. A significant reduction (for about 10 cm^{-1}) of the A_{1g} mode linewidth, as well as an increase of the B_{1g} mode linewidth (for about 2.4 cm^{-1}) is found in the $Fe_{1.02}Te_{0.6}Se_{0.4}$ sample. The A_{1g} mode hardening is a consequence of the replacement of heavier Te ions with lighter Se ions (the mass effect) and the unit-cell contraction (*c*-axis reduction) upon doping [26]. On the other hand, an introduction of substitutional impurities (disorder) should in general induce the linewidth increase in doped compounds [27], as it was observed for the B_{1g} mode. In the case of the A_{1g} mode, the phonon mode linewidth decrease can be related to the decrease of the electron–phonon interaction upon doping [28]. This assumption is also supported by the DFT calculations of the electron–phonon coupling constant λin the nonmagnetic solution, which shows a significant decrease of λ as the Te atoms are replaced with the Se atoms ($\lambda(FeTe)=0.30$ [29], $\lambda(FeTe_{0.5}Se_{0.5})=0.22$ [30], and $\lambda(FeSe)=0.17$ [31]). At this point we can not exclude the possibility that excess Fe ions may play role in the behaviour of the A_{1g} mode. The excess Fe ions are located within Te layer [32] and may produce qualitatively different effects from those induced by the substitutional disorder.

In the case of the B_{1g} mode (Fe ions vibrations) we expected the mode hardening due to the unit cell compression with doping by the Se atoms. Instead of the hardening, we observe the mode softening in the $Fe_{1.02}Te_{0.6}Se_{0.4}$ sample, which is in accordance with expectations for $FeTe_{1-x}Se_x$ solid solution based on a linear fit of the mode energy values of parent crystals FeTe (this work) and FeSe [33], see the inset of Fig. 2. However, one should also have in mind that the change in the excess iron concentration (decrease from $y=0.07$ for the undoped to $y=0.02$ for the 40% Se doped sample) may have significant impact on the B_{1g} mode energy [21].

Upon cooling, no additional Raman lines have been observed although the crystal structure and the crystal symmetry of FeTe are changed at $T<T_N$. By comparing the calculated phonon energies in both phases (see Table 1) it can be seen that the phonon energies do not differ substantially. In fact, the $E_g^1(E_g^2)$ mode of the tetragonal phase splits into $A_g^1/B_g^1(A_g^4/B_g^2)$ doublets of monoclinic symmetry, which appear at energies very close to the mode energies of tetragonal phase. In the case of the A_{1g} mode there is virtually no energy change between the A_{1g} mode of the tetragonal phase and the A_g^2 mode of the monoclinic phase (see Table 1). The B_{1g} mode of the tetragonal phase changes energy (softens) and symmetry (becomes A_g symmetry one) at the phase transition temperature. The change of the symmetry of this mode in the low temperature phase does not influence the low temperature Raman spectra because the energy of this mode (A_g^3) is far enough (40 cm^{-1}) from the (A_g^2) mode, preventing the phonon mode coupling between them [34]. The lattice vibration normal modes of the low temperature phase are given in Fig. 1(b).

Fig. 3 shows the energy and the linewidth temperature dependence for the A_{1g} and the B_{1g} modes of the $Fe_{1.07}Te$ sample, which are obtained from the Raman spectra measured at various temperatures using the Lorentzian profile fit. Solid and dashed lines in Fig. 3(c,d) are calculated curves obtained using the well known anharmonicity effect formula, [35,27] which takes into account three-phonon processes for the temperature dependent change of the phonon energy and linewidth:

$$\omega(T)=\omega_0-C[1+2/(e^x-1)], \quad (1)$$

$$\Gamma(T)=\Gamma_0+A[1+2/(e^x-1)], \quad (2)$$

where ω_0 (Γ_0) is the temperature independent energy (intrinsic linewidth), C (A) is the anharmonic constant and $x=\hbar\omega_0/(2k_BT)$. The best fit parameters are indicated in Fig. 3(c,d). A rather good agreement between the experimental data and fitted curves for the A_{1g} mode is observed in the whole temperature range (above and below $T_N=70$ K). Large value of Γ_0 parameter in comparison to the anharmonic constant ($24.5 \gg 1\ cm^{-1}$) also suggest the importance of the electron–phonon interaction for this mode [36] or the orbital degrees of freedom of Fe ions [20].

Upon cooling, the B_{1g} mode of the undoped sample shows pronounced broadening down to T_N, when it suddenly narrows (see Fig. 3(b)). This deviation from the standard anharmonic picture suggests the presence of additional scattering process. The energy and broadening temperature change of the B_{1g} mode closely follows the normalized magnetic susceptibility curve, as can be seen in Fig. 4, indicating that spin-phonon coupling leaves a

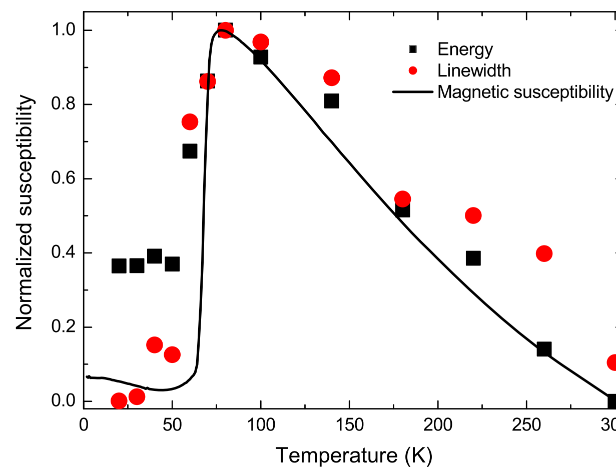

Fig. 4. (Color online) Temperature dependence of the normalized frequency and linewidth of the B_{1g} mode together with the normalized magnetic susceptibility (solid line) of $Fe_{1.07}Te$ single crystal.

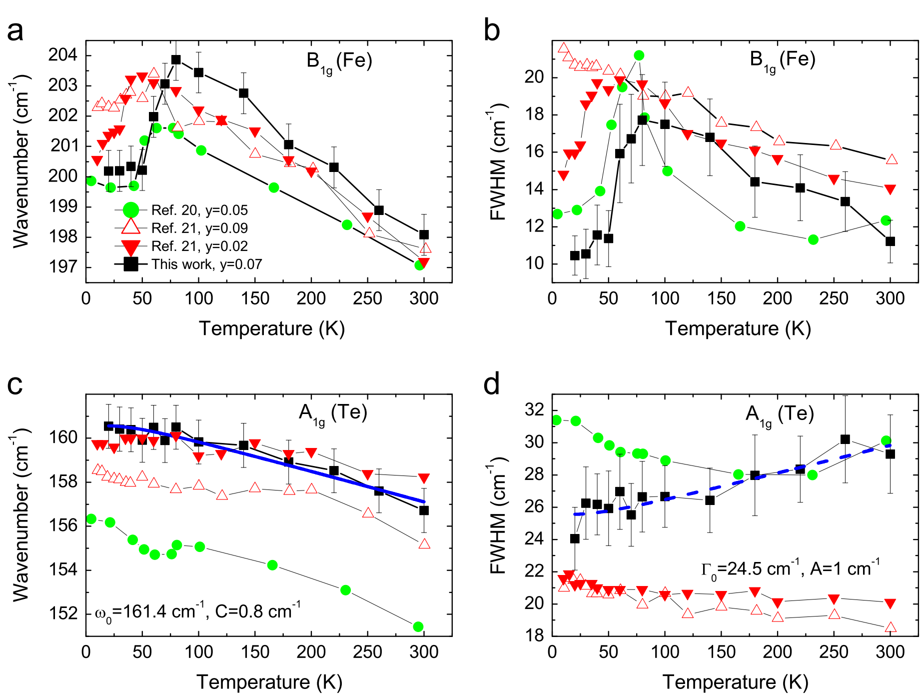

Fig. 3. (Color online) The phonon energy and the linewidth temperature dependence of the A_{1g} (c,d) and the B_{1g} (a,b) modes of $Fe_{1+y}Te$ single crystal together with existing literature data [20,21]. The solid and the dashed lines represent calculated curves using Eqs. (1) and (2), respectively.

fingerprint in the phonon dynamics of FeTe. This is to be expected because the B_{1g} mode represents vibrations of Fe-ions which carry the magnetic moments. Softening of the B_{1g} mode below T_N is a consequence of the antiferromagnetic ordering and structural change (see Table 1).

In the case of the $Fe_{1.02}Te_{0.6}Se_{0.4}$ sample, the temperature dependencies of the phonon mode energy and linewidth follow the standard anharmonic picture for both vibrational modes. The absence of the B_{1g} mode softening in this sample at temperatures below 70 K is a consequence of the suppression of antiferromagnetic ordering with doping [13].

Finally, in Fig. 3 we compared energy and linewidth vs temperature dependence of the A_{1g} and B_{1g} modes with previously published results [20,21]. The B_{1g} mode energy and linewidth (Fig. 3(a,b)) show no substantial difference from our results (taking into account that error bar in our case is $\pm 2\ cm^{-1}$; in Ref. [21] is $\pm 4\ cm^{-1}$) except of the position of *FWHM(T)* curve maximum, which is related to the sample composition, *i.e.*, T_N. The A_{1g} mode energy temperature dependencies follow the same trend (mode hardening) by the temperature lowering in Refs. [20,21] and in this work. The main difference is the linewidth change by the temperature lowering (Fig. 3(d)). We have shown that the linewidth narrows by temperature lowering, but an opposite trend is found in Refs. [20,21]. Our finding is in accordance with an anharmonic picture.

4. Conclusion

In summary, we have measured the Raman scattering spectra of the $Fe_{1+y}Te_{1-x}Se_x$ (x=0, y=0.07; x=0.1, y=0.05 and x=0.4, y=0.02) alloys at various temperatures. Two out of four Raman-active modes predicted by the factor-group analysis have been experimentally observed and assigned. Energies of these modes are in rather good agreement with our lattice dynamics calculations. The main focus of our work was the temperature and doping dependence of the phonon energies and linewidths, whose features are, to some extent, contradictory in previous works. We have shown that the A_{1g} mode (corresponding to the Te ions vibration along the z-axis) follows the standard anharmonic temperature dependence (which originates in the phonon–phonon interaction) both in the doped and the undoped samples. The width of the A_{1g} mode at room temperature is significantly reduced in the doped samples. In the case of the B_{1g} mode, the phonon frequency and the linewidth closely follow the magnetic susceptibility temperature dependence, indicating the presence of the spin-phonon coupling in the undoped $Fe_{1.07}Te$ sample. The antiferromagnetic ordering is suppressed by doping, and $Fe_{1.02}Te_{0.6}Se_{0.4}$ sample follows a conventional temperature dependence in both phonon modes.

Acknowledgments

This work was supported by the Serbian Ministry of Education, Science and Technological Development under Projects ON171032, ON171017 and III45018. Work at Brookhaven was supported by the US DOE under Contract No. DE-AC02-98CH10886 and in part by the Center for Emergent Superconductivity, an Energy Frontier Research Center funded by the US DOE, Office for Basic Energy Science (H.L. and C.P.). Numerical simulations were run on the AEGIS e-Infrastructure, supported in part by FP7 projects EGI-InSPIRE, and PRACE-3IP.

References

[1] H. Okada, Y. Takahashi, K. Igawa, K. Arii, H. Takahashi, T. Watanabe, H. Yanagi, Y. Kamihara, T. Kamiya, M. Hirano, H. Hosono, S. Nakano, T. Kikegawa, J. Phys. Soc. Jpn 77SC (Suppl. C) (2008) S119–S120.
[2] M.H. Yoichi Kamihara, Takumi Watanabe, H. Hosono, J. Am. Chem. Soc. 130 (2008) 3296 130 (11) (2008) 3296–3297.
[3] G.R. Stewart, Rev. Mod. Phys. 83 (2011) 1589–1652.
[4] F.-C. Hsu, J.-Y. Luo, K.-W. Yeh, T.-K. Chen, T.-W. Huang, P.M. Wu, Y.-C. Lee, Y.-L. Huang, Y.-Y. Chu, D.-C. Yan, M.-K. Wu, Proc. Natl. Acad. Sci. U.S.A. 105 (38) (2008) 14262–14264.
[5] Y. Mizuguchi, F. Tomioka, S. Tsuda, T. Yamaguchi, Y. Takano, Appl. Phys. Lett. 94 (1) (2009) 012503.
[6] M. Rotter, M. Tegel, D. Johrendt, I. Schellenberg, W. Hermes, R. Pöttgen, Phys. Rev. B 78 (2008) 020503.
[7] M. Rotter, M. Tegel, D. Johrendt, Phys. Rev. Lett. 101 (2008) 107006.
[8] J.H. Tapp, Z. Tang, B. Lv, K. Sasmal, B. Lorenz, P.C.W. Chu, A.M. Guloy, Phys. Rev. B 78 (2008) 060505.
[9] J. Guo, S. Jin, G. Wang, S. Wang, K. Zhu, T. Zhou, M. He, X. Chen, Phys. Rev. B 82 (2010) 180520.
[10] N. Lazarević, M. Abeykoon, P.W. Stephens, H. Lei, E.S. Bozin, C. Petrovic, Z. V. Popović, Phys. Rev. B 86 (2012) 054503.
[11] K.-W. Yeh, T.-W. Huang, Y. lin Huang, T.-K. Chen, F.-C. Hsu, P.M. Wu, Y.-C. Lee, Y.-Y. Chu, C.-L. Chen, J.-Y. Luo, D.-C. Yan, M.-K. Wu, Europhys. Lett. 84 (3) 37002.
[12] S. Li, C. delaCruz, Q. Huang, Y. Chen, J.W. Lynn, J. Hu, Y.-L. Huang, F.-C. Hsu, K.-W. Yeh, M.-K. Wu, P. Dai, Phys. Rev. B 79 (2009) 054503.
[13] C.-Y. Moon, H.J. Choi, Phys. Rev. Lett. 104 (2010) 057003.
[14] M.H. Fang, H.M. Pham, B. Qian, T.J. Liu, E.K. Vehstedt, Y. Liu, L. Spinu, Z.Q. Mao, Phys. Rev. B 78 (2008) 224503.
[15] Y. Mizuguchi, F. Tomioka, S. Tsuda, T. Yamaguchi, Y. Takano, Appl. Phys. Lett. 93 (15) (2008) 152505.
[16] I.I. Mazin, Nature 464 (2010) 183–186.
[17] T. Bazhirov, M.L. Cohen, Phys. Rev. B 86 (2012) 134517.
[18] T.-L. Xia, D. Hou, S.C. Zhao, A.M. Zhang, G.F. Chen, J.L. Luo, N.L. Wang, J.H. Wei, Z.-Y. Lu, Q.M. Zhang, Phys. Rev. B 79 (2009) 140510.
[19] K. Okazaki, S. Sugai, S. Niitaka, H. Takagi, Phys. Rev. B 83 (2011) 035103.
[20] V. Gnezdilov, Y. Pashkevich, P. Lemmens, A. Gusev, K. Lamonova, T. Shevtsova, I. Vitebskiy, O. Afanasiev, S. Gnatchenko, V. Tsurkan, J. Deisenhofer, A. Loidl, Phys. Rev. B 83 (2011) 245127.
[21] Y.J. Um, A. Subedi, P. Toulemonde, A.Y. Ganin, L. Boeri, M. Rahlenbeck, Y. Liu, C. T. Lin, S.J.E. Carlsson, A. Sulpice, M.J. Rosseinsky, B. Keimer, M. Le Tacon, Phys. Rev. B 85 (2012) 064519.
[22] H. Lei, R. Hu, E.S. Choi, J.B. Warren, C. Petrovic, Phys. Rev. B 81 (2010) 094518.
[23] S. Baroni, S. de Gironcoli, A. Dal Corso, P. Giannozzi, Rev. Mod. Phys. 73 (2001) 515–562.
[24] P. Giannozzi, S. Baroni, N. Bonini, M. Calandra, R. Car, C. Cavazzoni, D. Ceresoli, G.L. Chiarotti, M. Cococcioni, I. Dabo, A.D. Corso, S. de Gironcoli, S. Fabris, G. Fratesi, R. Gebauer, U. Gerstmann, C. Gougoussis, A. Kokalj, M. Lazzeri, L. Martin-Samos, N. Marzari, F. Mauri, R. Mazzarello, S. Paolini, A. Pasquarello, L. Paulatto, C. Sbraccia, S. Scandolo, G. Sclauzero, A.P. Seitsonen, A. Smogunov, P. Umari, R.M. Wentzcovitch, J. Phys. Condens. Matter 21 (39) 395502.
[25] A. Martinelli, A. Palenzona, M. Tropeano, C. Ferdeghini, M. Putti, M. R. Cimberle, T.D. Nguyen, M. Affronte, C. Ritter, Phys. Rev. B 81 (2010) 094115.
[26] K. Horigane, H. Hiraka, K. Ohoyama, J. Phys. Soc. Jpn 78 (7) (2009) 074718.
[27] M. Cardona, T. Ruf, Solid State Commun. 117 (3) (2001) 201–212.
[28] N. Lazarević, Z.V. Popović, R. Hu, C. Petrovic, Phys. Rev. B 81 (2010) 144302.
[29] J. Li, G. Huang, X. Zhu, Physica C 492 (2013) 152–157.
[30] J. Li, G. Huang, Solid State Commun. 159 (2013) 45–48.
[31] A. Subedi, L. Zhang, D.J. Singh, M.H. Du, Phys. Rev. B 78 (2008) 134514.
[32] W. Bao, Y. Qiu, Q. Huang, M.A. Green, P. Zajdel, M.R. Fitzsimmons, M. Zhernenkov, S. Chang, M. Fang, B. Qian, E.K. Vehstedt, J. Yang, H. M. Pham, L. Spinu, Z.Q. Mao, Phys. Rev. Lett. 102 (2009) 247001.
[33] V. Gnezdilov, Y.G. Pashkevich, P. Lemmens, D. Wulferding, T. Shevtsova, A. Gusev, D. Chareev, A. Vasiliev, Phys. Rev. B 87 (2013) 144508.
[34] N. Lazarević, M.M. Radonjić, D. Tanasković, R. Hu, C. Petrovic, Z.V. Popović, J. Phys. Condens. Matter 24 (25) 255402.
[35] M. Balkanski, R.F. Wallis, E. Haro, Phys. Rev. B 28 (1983) 1928–1934.
[36] A.P. Litvinchuk, B. Lv, C.W. Chu, Phys. Rev. B 84 (2011) 092504.